Supplementary information:

Selective Pd recovery from Acidic Leachates by 3-Mercaptopropylphosphonic Acid grafted TiO_2: Does Surface Coverage Correlate to Performance?

Nick Gys[a,b], Bram Pawlak[c], Léon Luntadila Lufungula[d], Kristof Marcoen[e], Kenny Wyns[a], Kitty Baert[e], Thomas Abo Atia[a,f], Jeroen Spooren[a], Peter Adriaensens[c], Frank Blockhuys[d], Tom Hauffman[e], Vera Meynen[a,b], Steven Mullens[a], Bart Michielsen[a]

[a]Sustainable Materials, Flemish Institute for Technological Research (VITO NV), Boeretang 200, 2400 Mol, Belgium.

[b]Laboratory of Adsorption and Catalysis (LADCA), Department of Chemistry, University of Antwerp, Universiteitsplein 1, 2610 Wilrijk, Belgium.

[c]Analytical and Circular Chemistry (ACC), Institute for Materials Research (IMO), Hasselt University, Agoralaan 1, 3590 Diepenbeek, Belgium.

[d]Structural Chemistry Group, Department of Chemistry, University of Antwerp, Groenenborgerlaan 171, 2020 Antwerp, Belgium.

[e]Research Group Electrochemical and Surface Engineering (SURF), Department Materials and Chemistry, Vrije Universiteit Brussel, Pleinlaan 2, 1050 Brussels, Belgium

[f]Department of Chemistry, KU Leuven, Celestijnenlaan 200F, 3000 Leuven, Belgium

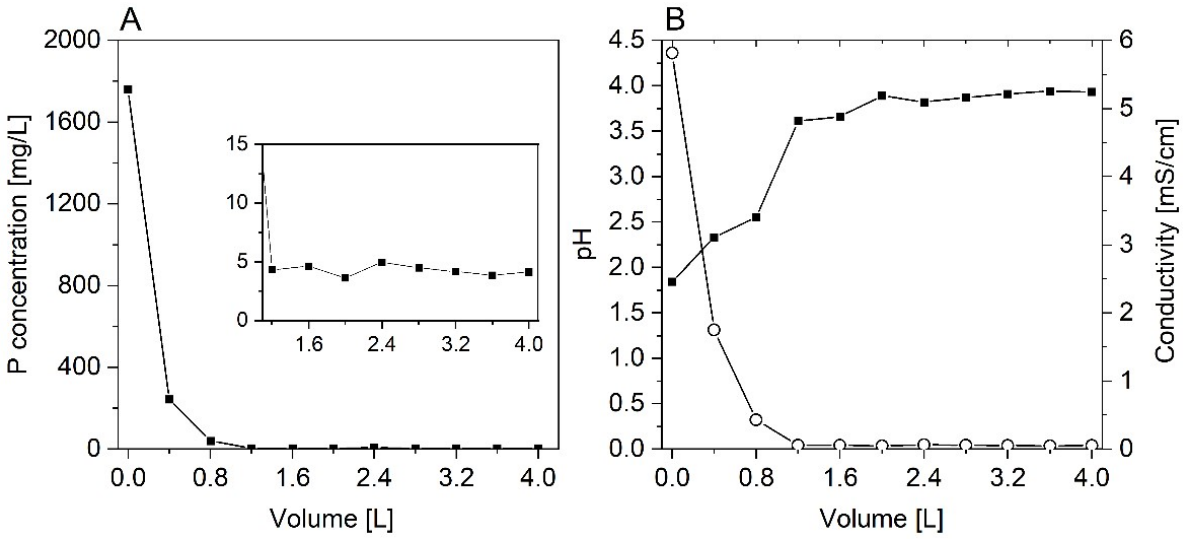

Figure S.1: Evolution of the phosphorus concentration (A) and pH and conductivity (B) during pressure filtration of 3MPPA150. Squares (pH), open circles (conductivity).

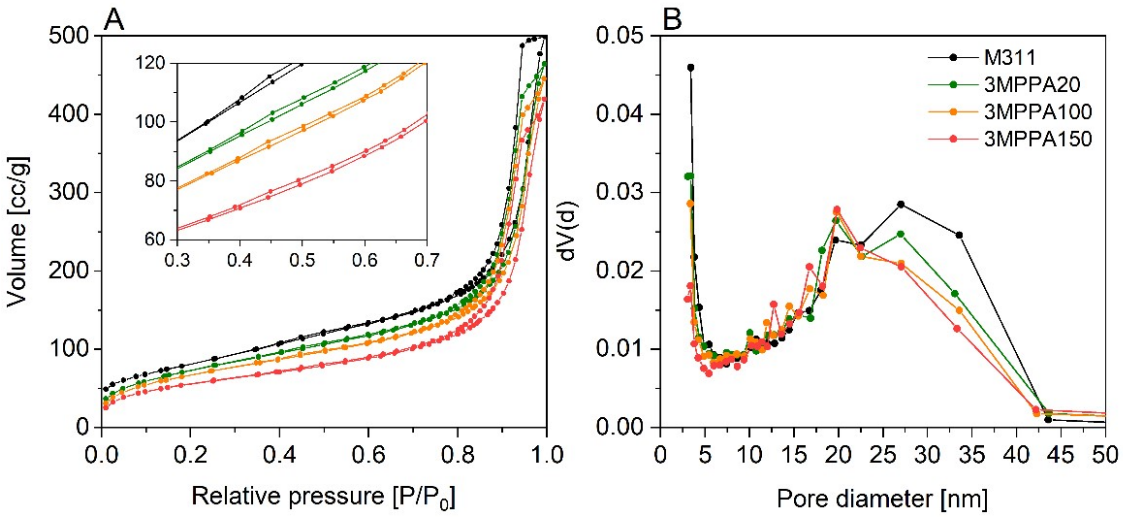

Figure S.2: N_2 adsorption-desorption isotherms (A) and BJH pore size distribution (B) calculated from the desorption branch of unmodified M311 and 3MPPA modified M311.

Table S.1: Physicochemical properties of native Hombikat M311 and 3MPPA modified Hombikat M311, derived from N_2 sorption.

Sample	S_{BET} (m^2/g)	V_{pore} (cm^3/g)	C constant
Hombikat M311	300	0.695	91
3MPPA20	270	0.661	53
3MPPA50	260	0.631	53
3MPPA100	250	0.631	52
3MPPA150	207	0.614	60

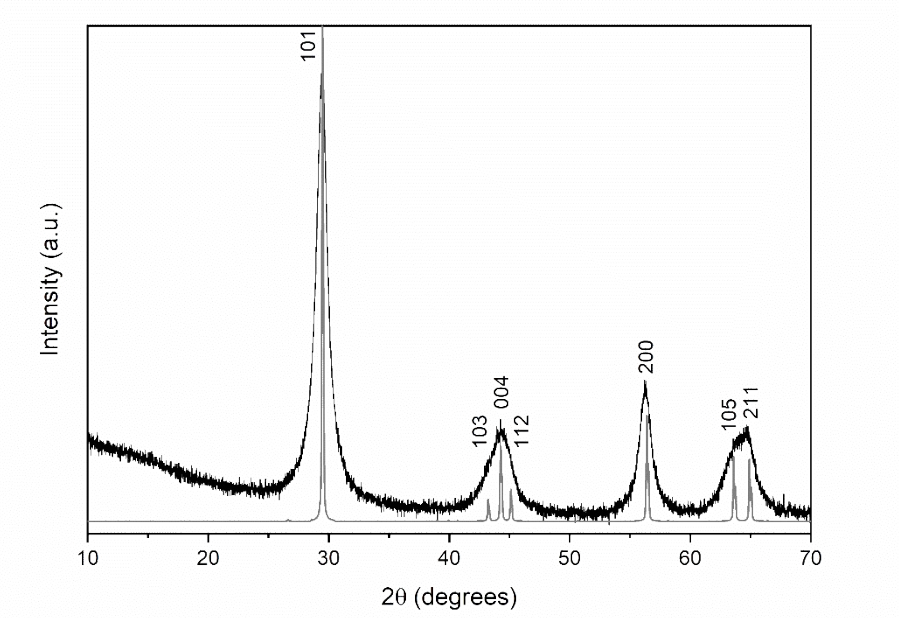

Figure S.3: Powder XRD pattern of Hombikat M311 with diffraction peaks of anatase.

Table S.2: Calculation of the 004/101 crystal facet ratio based on the area of the corresponding diffraction peaks.

Crystal facet	2theta (°)	FWHM (°)	d – spacing (Å)	Area	004 / 101
101	29.407	1.089	3.524	8185.16	12%
004	44.192	1.701	2.378	953.26	

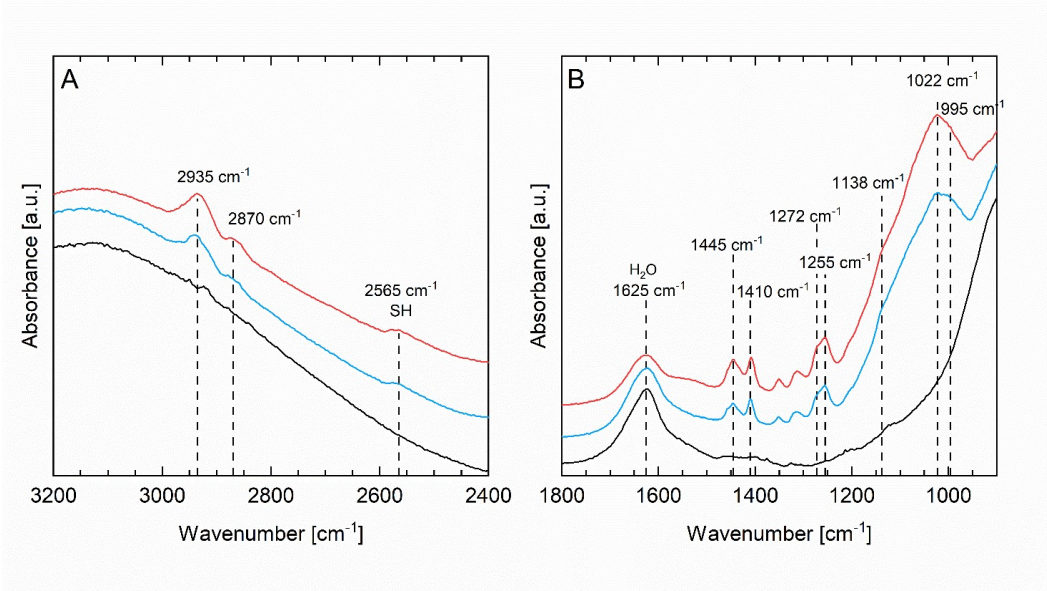

Figure S.4: DRIFT spectra of unmodified Hombikat M311 (black), 3MPPA50 (blue) and 3MPPA150 (red) recorded after 30 minutes under low vacuum (30 mbar). A: region 3200 cm^{-1} to 2400 cm^{-1}, B: region 1800 cm^{-1} to 900 cm^{-1}.

In the alkyl stretching region between 3000 and 2800 cm^{-1}, two broad signals are present at 2935 and 2870 cm^{-1} which can be assigned to the asymmetric and symmetric vibrations of the methylene groups, respectively.[1,2] The broadening of these signals is related to the different chemical environments of each methylene group, resulting in small differences in their peak position. The different chemical environment of each methylene group is well-illustrated in the relative positions of their deformation vibration signals. The signal at 1410 cm^{-1} can be assigned to CH_2- bound to P, while the signal at 1445 cm^{-1} is assigned to CH_2- bound to the SH functional group. The deformation vibration of the central methylene group is present as a shoulder at 1455 cm^{-1}.[1]

Furthermore, large similarities in the P-O region[3] between 1300 and 900 cm^{-1} are found, which is characterized by a superposition of at least three absorption bands at 1138, 1022 and 995 cm^{-1}. In the region between 1300 and 1200 cm^{-1}, two signals are visible at 1272 and 1255 cm^{-1} with similar relative intensities and broadness in both samples. In previous studies, signals located in this region were commonly assigned to the P=O stretching vibration.[4–7] However, computational studies point to the fact that, irrespective of the binding mode (mono -, bi- or tridentate), PA grafting involves coordination

of the P=O group towards a surface Ti atom resulting in a considerable shift of the P=O vibration to lower wavenumbers.[8] Consequently, the assignment of these signals and their correlation to a precise binding mode remains uncertain.

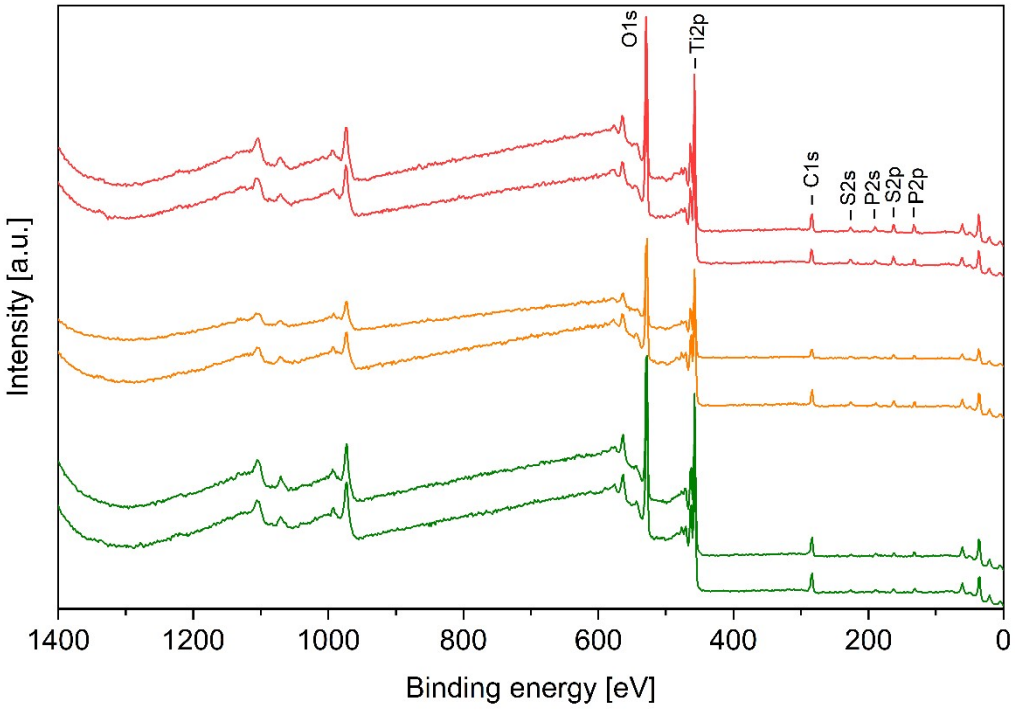

Figure S.5: XPS survey of 3MPPA20 (green), 3MPPA100 (orange) and 3MPPA150 (red). Two spectra were acquired for each sample.

Table S.3: Atomic concentrations* of C, O, P, S and Ti in 3MPPA20, 3MPPA100 and 3MPPA150 based on XPS. *two measurements were performed for each sample.

Sample	C (%)	O (%)	P (%)	S (%)	Ti (%)
3MPPA20	17.9	56.7	1.7	1.2	22.6
	16.5	57.8	1.6	1.3	22.9
3MPPA100	17.0	56.0	2.7	2.4	21.9
	16.0	56.9	2.8	2.4	22.1
3MPPA150	15.0	57.3	3.2	2.9	21.6
	15.6	56.8	3.2	2.8	21.6

Table S.3 depicts the calculated atomic concentrations of C, O, P, S and Ti of 3MPPA20, 3MPPA100 and 3MPPA150, based on two measurements for each sample. Data analysis was performed with the PHI Multipak software package, using the database-provided relative sensitivity factors of each element. With increasing 3MPPA concentration during grafting, an increasing atomic concentration of P and S is observed.

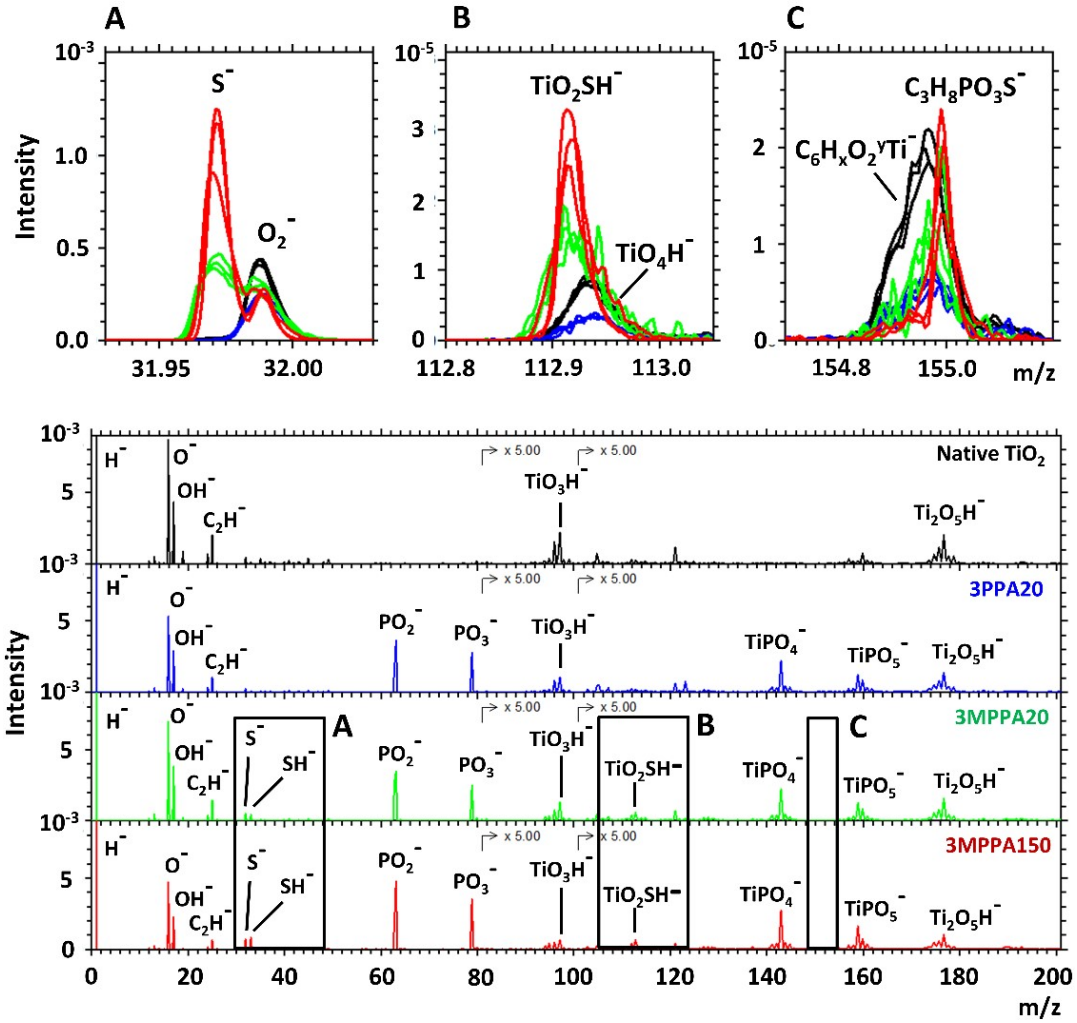

Figure S.6: Negative ToF-SIMS spectra overlay (0-200 m/z) of Hombikat M311 (black), 3PPA20 (blue), 3MPPA20 (green) and 3MPPA150 (red), with a detailed spectra overlay of the S^- (A), TiO_2SH^- (B) and $C_3H_8PO_3S^-$ (C) ion fragments. The spectra are normalized to the total ion intensity. *3PPA is a propylphosphonic acid modified reference sample*

Table S.4: DFT calculated adsorption energies (kJ/mol) and ^{31}P chemical shifts (ppm) of a selection of different surface conformations of 3MPPA on clean anatase (101). M indicates monodentate structures, B bidentate structures.

Conformation	**Binding mode**	**Adsorbate Interaction**	**E_{ads} (kJ/mol)**	**^{31}P shift (ppm)**
1	M	Free SH	-227.92	21.5
2	B	Free SH	-238.82	26.5
3	M	Intra S-H…O	-225.25	25.5
4	M	Inter S-H…O	-239.49	21.2 and 26.2
5	M	Inter S-H…O	-241.46	20.3 and 29.9
6	M	Inter S-H…S	-239.49	21.1 and 26.0
6*	M	**6** with no interaction	-238.24	22.4 and 22.4
7	B	Inter S-H…S	-268.42	27.8 and 32.9
7*	B	**7** with no interaction	-256.86	28.9 and 29.2
8	M	SH…Ti	-264.02	26.2
9	M	S…Ti	-222.75	30.9
10	B	SH…Ti	-286.96	26.9
11	B	S…Ti	-227.92	30.1

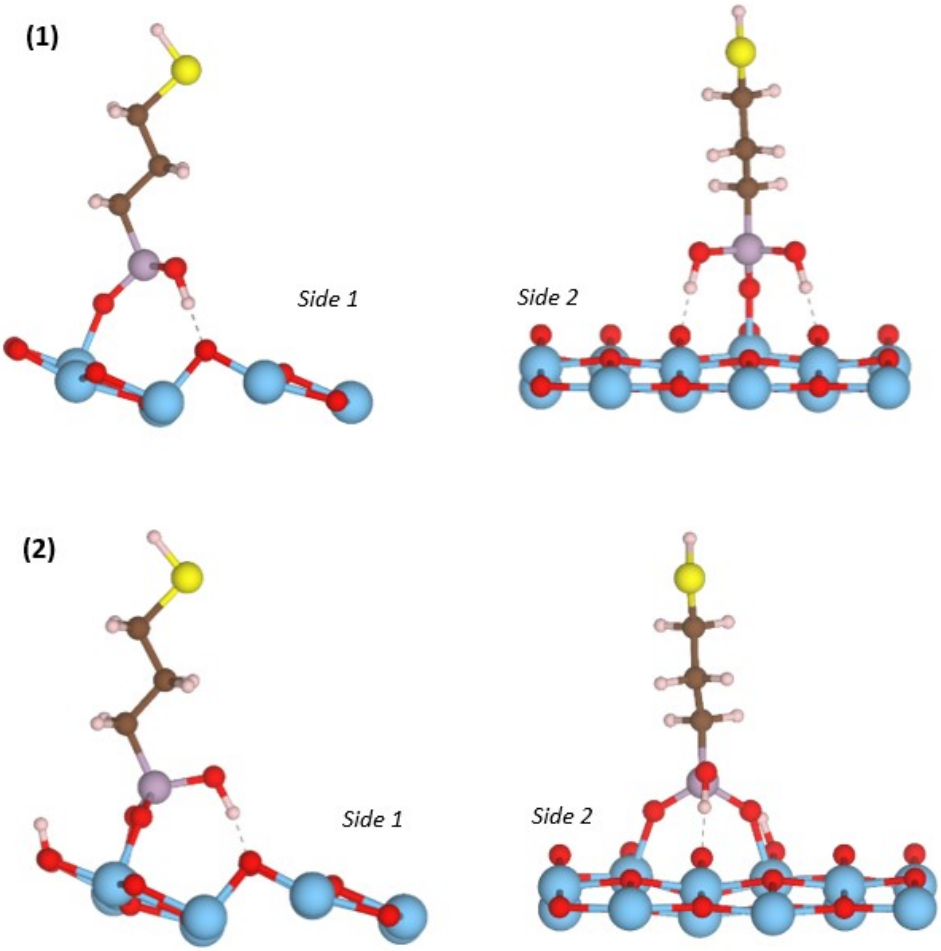

Figure S.7: Examples of optimized calculated geometries of the monodentate (1) and bidentate structures (2) of 3MPPA adsorbed on anatase (101) with free, non-interacting SH groups. Red, cyan, pink, brown, white and yellow represent oxygen, titanium, phosphorus, carbon, hydrogen and sulfur atoms, respectively.

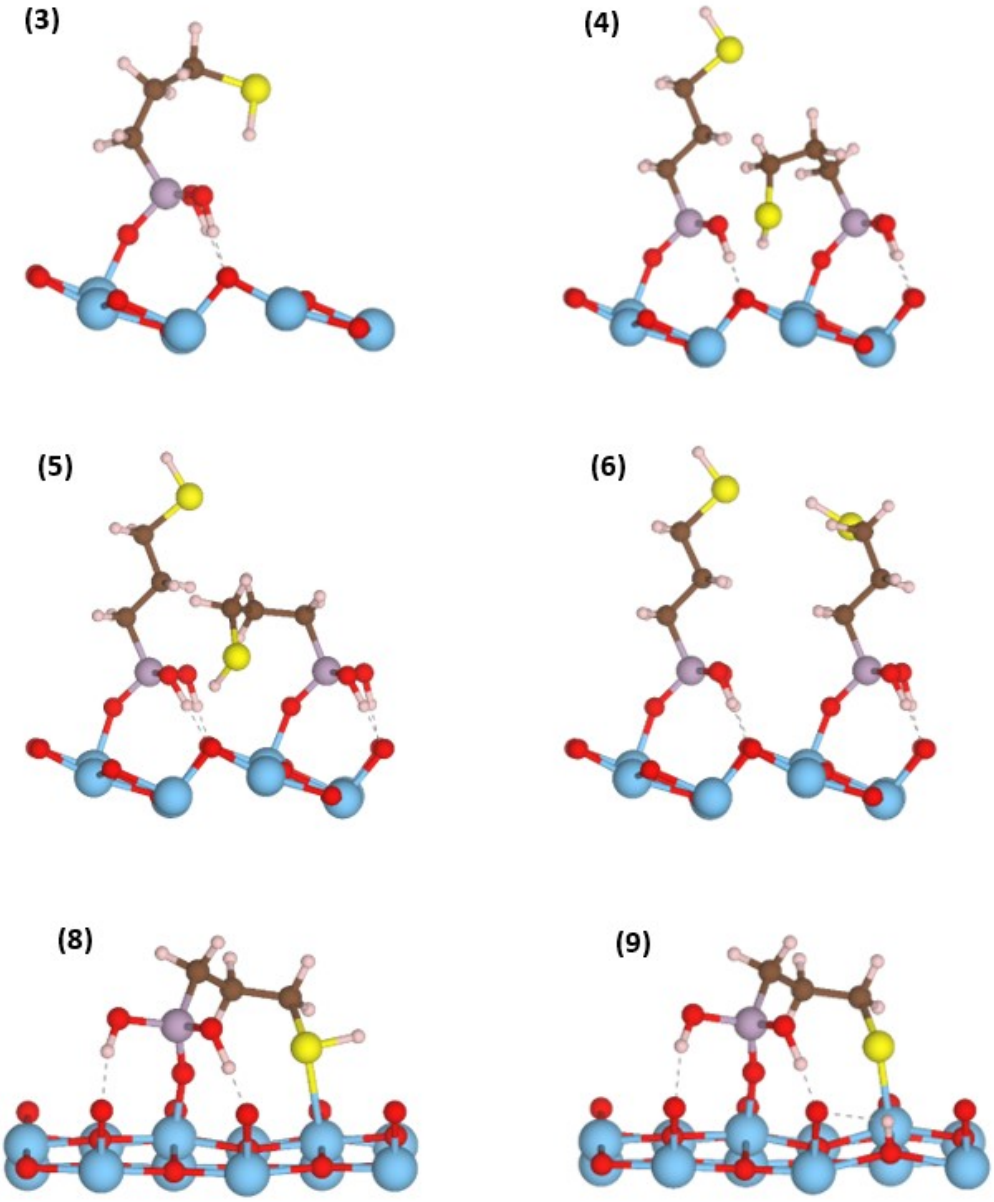

Figure S.8: Examples of optimized calculated geometries of 3MPPA adsorbed on anatase (101) of the intra-adsorbate S–H…O interaction (3), the inter-adsorbate S–H…O interaction (4-5), the inter-adsorbate S–H…S interaction (6), the non-dissociative SH…Ti interaction (8) and the dissociative S…Ti interaction (9). Red, cyan, pink, brown, white and yellow represent oxygen, titanium, phosphorus, carbon, hydrogen and sulfur atoms, respectively.

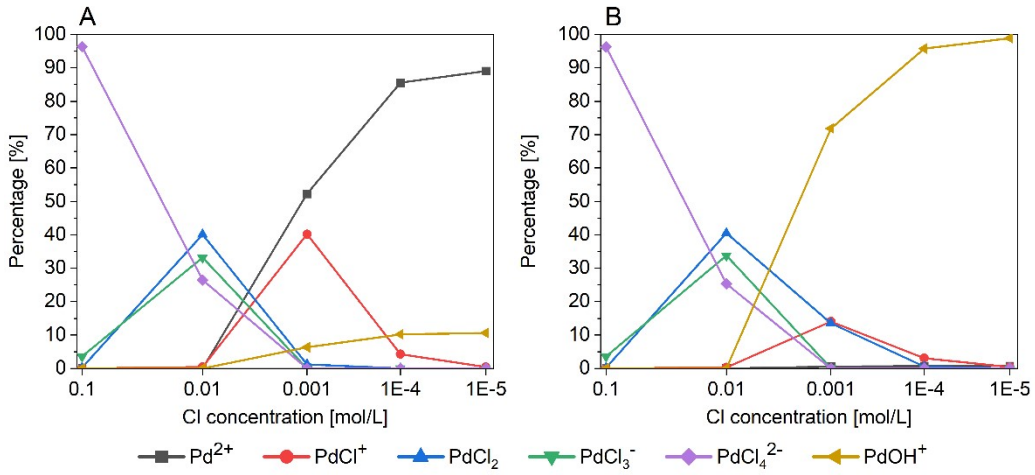

Figure S.9: Impact of chlorine concentration (10^{-1}-10^{-5} mol/L) on the palladium speciation at pH 2 (A) and pH 5 (B). Speciation modelling was performed using Visual MINTEQ software.

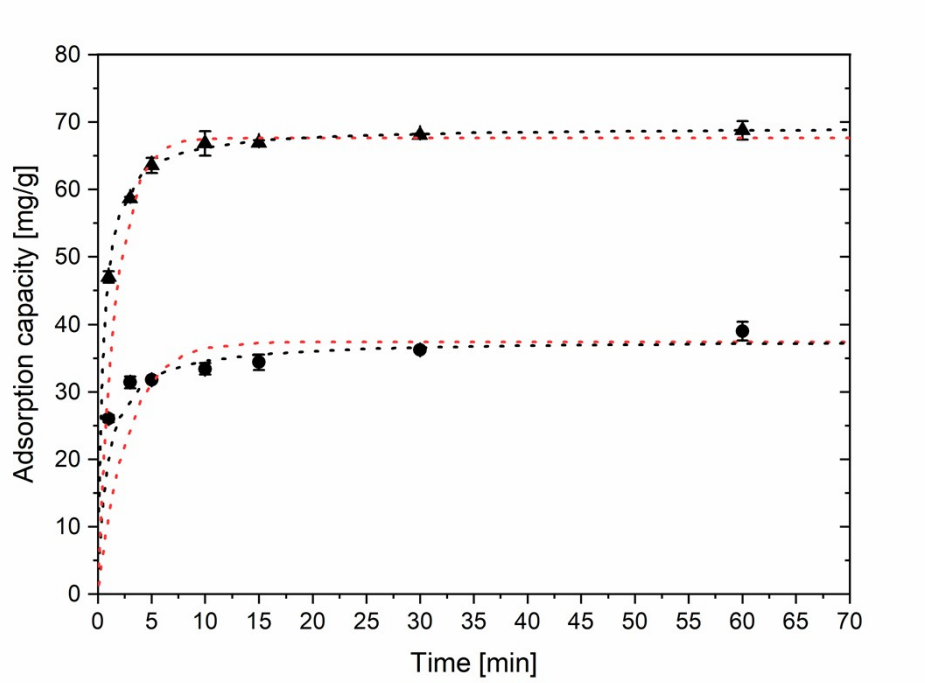

Figure S.10: Plot of non-linear pseudo first-order fit (dashed red line) and pseudo-second order fit (dashed black line) and experimental data points for the Pd adsorption kinetics for 3MPPA20 (closed circles) and 3MPPA150 (triangles). C_{Pd} = 250 mg/L, adsorbent dose = 2.5 g/L, pH = 2.0

Table S.5: Calculated S…S distances for adjacent 3MPPA groups on anatase (101) in their SH…S inter-adsorbate - and non-interacting conformation. M: monodentate, B: bidentate

Binding mode	**Adsorbate Interaction**	**S…S distance (Å)**
M	Inter SH…S	3.88
M	Non-interacting	5.58
B	Inter SH…S	3.79
B	Non-interacting	4.92

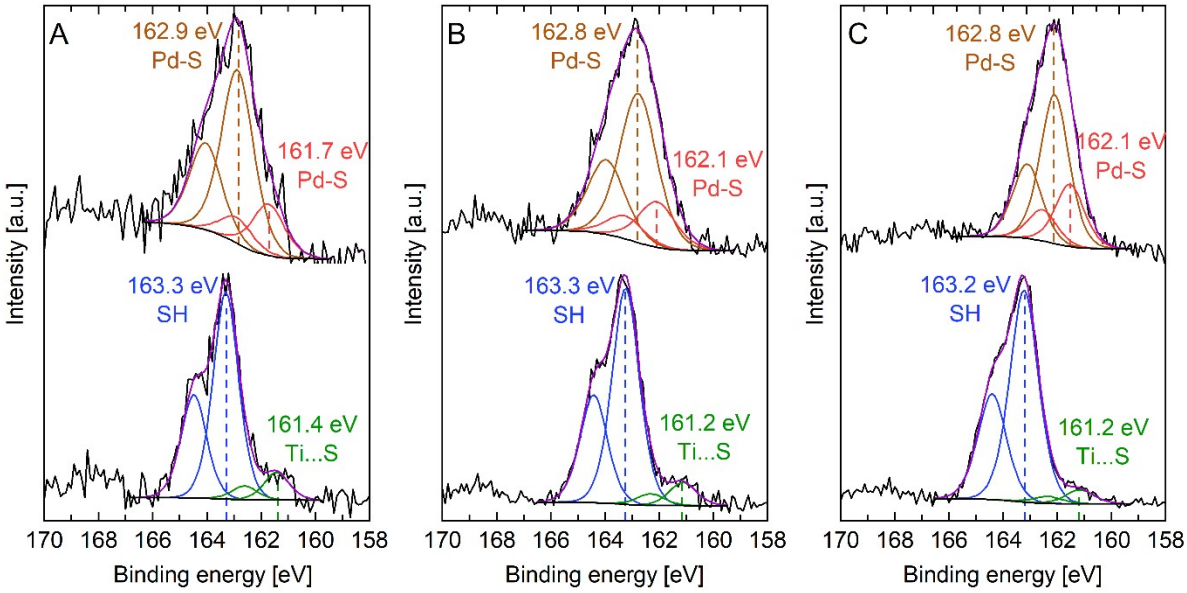

Figure S.11: S 2p XPS spectra of the as-synthesized (bottom) and Pd-loaded 3MPPA modified Hombikat M311 adsorbents (top): 3MPPA20 (A), 3MPPA100 (B) and 3MPPA150 (C).

Upon palladium adsorption, the S2p spectra are broadened and shifted to lower binding energies for all modification degrees.[9,10] As mentioned and rationalized in the main article, only the peak positions of the $S2p_{3/2}$ spin component are discussed. Peak fitting results in two components and implies the presence of two chemical states of sulfur upon palladium adsorption, with a predominant $S2p_{3/2}$ signal at a binding energy between 162.9-162.8 eV for each modification degree (brown dotted lines). A shift to lower binding energy is observed compared to the $S2p_{3/2}$ signal between 163.3-163.2 eV for free thiol functional groups (blue dotted lines).[9] At lower binding energies, a second component is visible with a $S2p_{3/2}$ signal between 161.7-162.1 eV (red dotted lines).

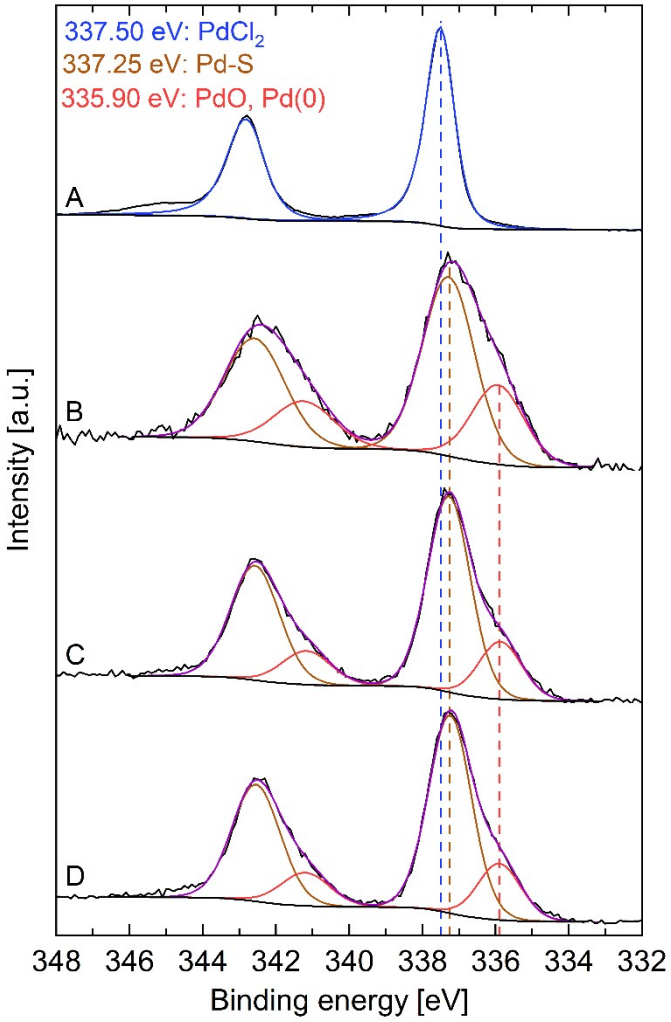

Figure S.12: Pd 3d XPS spectra of $PdCl_2$ (A) and Pd-loaded 3MPPA modified Hombikat M311 adsorbents: 3MPPA20 (B), 3MPPA100 (C) and 3MPPA150 (D).

Pd 3d XPS spectra typically consist of well-resolved Pd $3d_{5/2}$ and Pd $3d_{3/2}$ spin doublet peaks with a 5.30 eV splitting in binding energy[11], and similarly to S 2p, the most intense spin component (i.e. Pd $3d_{5/2}$) is typically used for discussion and interpretation. The Pd $3d_{5/2}$ signal in solid Pd(II)Cl_2 at a binding energy of 337.50 eV has been used as reference to clearly allocate changes in binding energy and chemical state(s) of Pd upon sorption. In the corresponding spectra of the Pd loaded samples, two components can be identified upon peak fitting. A first component with a Pd $3d_{5/2}$ signal at a binding energy of 337.25 eV confirms the binding between sulfur and palladium.[9,12] A second component is present at a binding energy of 335.90 eV which is indicative for palladium oxides or palladium hydroxides, which might have formed via partial hydrolysis and/or oxidation of Pd-S bonds during the material drying step (60 °C) after sorption.[13] Alternatively, this component can be assigned to Pd(0) species formed during the XPS measurement as palladium is reduced rapidly by X-rays.[14]

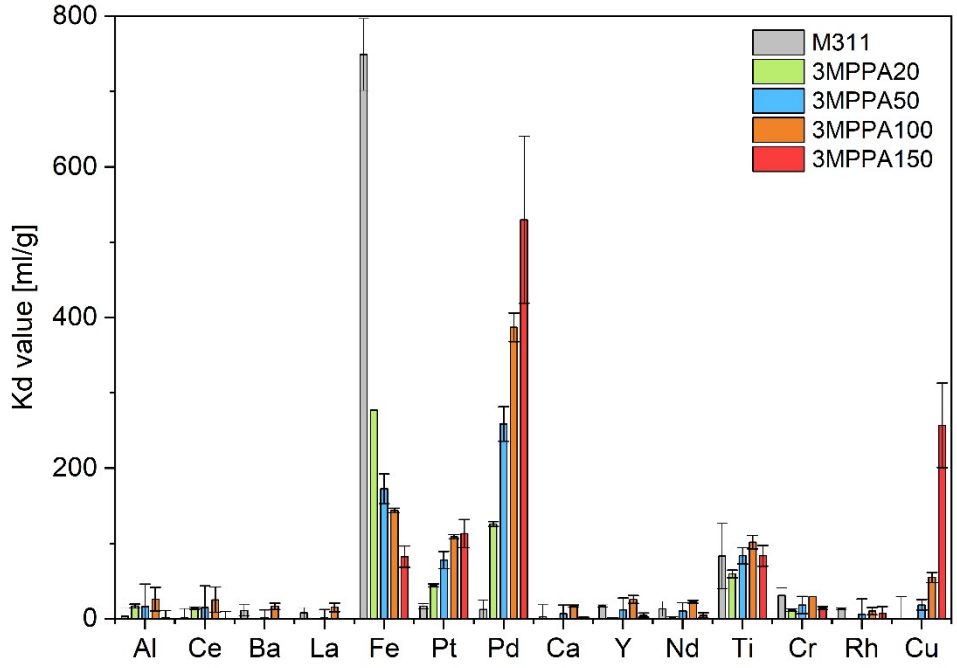

Figure S.13: Distribution coefficient values (K_d) for metals present in the automotive catalyst acidic leachate upon adsorption with native Hombikat M311 and 3MPPA grafted Hombikat M311 at the different surface coverages.

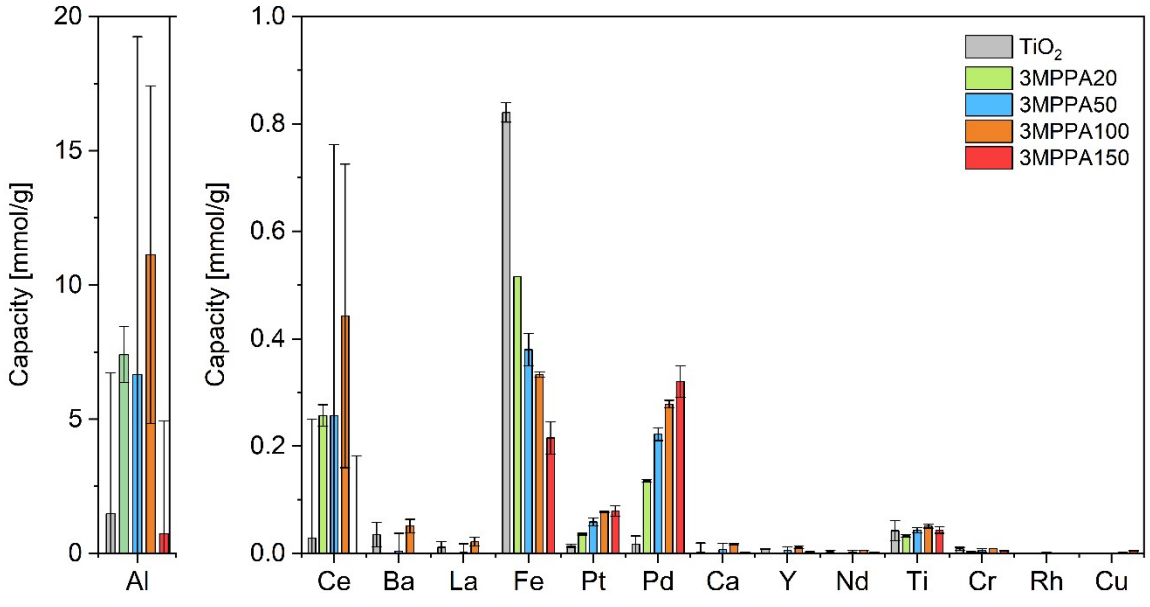

Figure S.14: Adsorption capacities (Q_d) for metals present in the automotive catalyst acidic leachate upon adsorption with native Hombikat M311 and 3MPPA grafted Hombikat M311 at the different surface coverages.

Table S.6: Calculated separation factors (SF) of Pd relative to Pt, Fe and Cu for the different surface coverages of 3MPPA after adsorption experiments with the automotive catalyst acidic leachate.* no adsorption of Cu at this surface coverage.

Surface coverage	SF (Pd/Pt)	SF (Pd/Fe)	SF (Pd/Cu)
0.9 #/nm²	2.8 ± 0.1	0.5 ± 0.0	*
1.3 #/nm²	3.3 ± 0.6	1.5 ± 0.2	14.0 ± 5.6
1.4 #/nm²	3.6 ± 0.2	2.7 ± 0.1	7.1 ± 0.9
1.9 #/nm²	4.7 ± 1.2	6.4 ± 1.7	2.1 ± 0.6

References

1. Socrates, G. *Infrared and Raman characteristic group frequencies*. *Infrared and Raman characteristic group frequencies* (2004). doi:10.1002/jrs.1238
2. Feichtenschlager, B., Lomoschitz, C. J. & Kickelbick, G. Tuning the self-assembled monolayer formation on nanoparticle surfaces with different curvatures: Investigations on spherical silica particles and plane-crystal-shaped zirconia particles. *J. Colloid Interface Sci.* **360**, 15–25 (2011).
3. Steiner, G. *et al.* Characterization of self assembly layers of octadecanephosphonic acid by polarisation modulation FT-IRRA spectroscopy mapping. *J. Mol. Struct.* **661**–**662**, 429–435 (2003).
4. Gao, W., Dickinson, L., Grozinger, C., Morin, F. G. & Reven, L. Self-Assembled Monolayers of Alkylphosphonic Acids on Metal Oxides. *Langmuir* **12**, 6429–6435 (1996).
5. Guerrero, G., Mutin, P. H. & Vioux, A. Organically modified aluminas by grafting and sol-gel processes involving phosphonate derivatives. *J. Mater. Chem.* **11**, 3161–3165 (2001).
6. Hotchkiss, P. J., Malicki, M., Giordano, A. J., Armstrong, N. R. & Marder, S. R. Characterization of phosphonic acid binding to zinc oxide. *J. Mater. Chem.* **21**, 3107 (2011).
7. Yah, W. O., Takahara, A. & Lvov, Y. M. Selective Modification of Halloysite Lumen with Octadecyl Phosphonic Acid : New Inorganic Tubular Micelle Selective. *J. Am. Chem. Soc.* **134**, 1853–1859 (2012).
8. Geldof, D. *et al.* Binding modes of phosphonic acid derivatives adsorbed on TiO2surfaces: Assignments of experimental IR and NMR spectra based on DFT/PBC calculations. *Surf. Sci.* **655**, 31–38 (2017).
9. McEleney, K., Crudden, C. M. & Horton, J. H. X-ray photoelectron spectroscopy and the auger parameter as tools for characterization of silica-supported pd catalysts for the suzuki-miyaura reaction. *J. Phys. Chem. C* **113**, 1901–1907 (2009).
10. Corthey, G., Rubert, A. A., Benitez, G. A., Fonticelli, M. H. & Salvarezza, R. C. Electrochemical and X-ray photoelectron spectroscopy characterization of Alkanethiols adsorbed on palladium surfaces. *J. Phys. Chem. C* **113**, 6735–6742 (2009).
11. Kostanovskiy, I., Schumann, F. O., Aliaev, Y., Wei, Z. & Kirschner, J. Core-resonant double photoemission from palladium films. *J. Phys. Condens. Matter* **28**, 15601 (2016).
12. Hanif, M. A., Ebralidze, I. I. & Horton, J. H. Pd and S binding energies and Auger parameters on a model silica-supported Suzuki-Miyaura catalyst: Insights into catalyst activation. *Appl. Surf. Sci.* **280**, 836–844 (2013).
13. Dobrzyńska, J., Dobrowolski, R., Olchowski, R., Zięba, E. & Barczak, M. Palladium adsorption and preconcentration onto thiol- and amine-functionalized mesoporous silicas with respect to analytical applications. *Microporous Mesoporous Mater.* **274**, 127–137 (2019).
14. Narayana, M., Michalik, J., Contarini, S. & Kevan, L. Determination of the chemical state of palladium in PdNa-X zeolite by Electron Spin Resonance and X-ray Photoelectron Spectroscopy. *J. Phys. Chem.* **89**, 3895–3899 (1985).